ORIGINAL PAPER

Debris flow disaster risk analysis and modeling via numerical simulation and land use assessment

Jun Wang [1,2,3] · Yan Yu [4] · Qinghua Gong [1,2,3] · Shaoxiong Yuan [1,2,3]

Abstract

To mitigate the risk of debris flows, quantitative risk assessments for different land use types are quite significant. However, with respect to debris flows, no sound relationship has so far been established between risks and different land use types. This study developed a method of debris flow risk assessment by incorporating numerical simulations with land use types. First, the key debris flow intensities for different return periods, including movement velocities and maximum flow depths, were identified via numerical simulations. Second, a debris flow hazard classification model based on a combination of the debris flow intensity and the return period was established to assess debris flow hazard degree. Then, the land use distribution within the inundated areas was itemized via the interpretation of remote sensing and field surveys, and the debris flow vulnerability was determined by the degree of functional damage or the cost of recovery of land uses caused under a given hazard. Finally, the potential debris flow risk zones were identified and mapped by combining debris flow hazard and vulnerability. The methodology was applied and verified in a small debris flow watershed in China. The proposed methodology can be performed effectively to conduct debris flow risk analysis and can be widely employed for debris flow mitigation.

Keywords Debris flow · Inundation simulation · Land use · Risk assessment · Disaster mitigation

Highlights

(1) Numerical simulations combined with land utilization data to perform debris flow disaster risk analysis and modeling.

(2) A debris flow hazard classification model on the basis of a combination of the debris flow intensity and the recurrence period was established.

(3) The quantitative relationship between debris flow vulnerability and 12 first-class land use classes.

✉ Yan Yu
yuyan10@mails.ucas.ac.cn

1   Guangdong Open Laboratory of Geospatial Information Technology and Application, Guangzhou 510070, China

2   Southern Marine Science and Engineering Guangdong Laboratory, Guangzhou 511458, China

3   Guangzhou Institute of Geography, Guangzhou 510070, China

4   Science and Technology Library of Guangdong Province, Guangdong Institute of Scientific & Technical Information and Development Strategy, Guangzhou 510070, China

Introduction

Debris flows generally consist of mixtures of water, sediment, wood, and fragmental materials and propagate rapidly along mountain slopes and channels causing serious losses of life and property (Gregoretti et al. 2016). Debris flows have occurred in more than 70 countries around the world and have recently become an important issue (Imaizumi et al. 2006; Dahal et al. 2009; Tecca and Genevois 2009; Cui et al. 2011; McCoy et al. 2012; Degetto et al. 2015; Tiranti and Deangeli 2015; Hu et al. 2016). For example, a large-scale debris flow induced by a rainstorm on August 7, 2010, in Zhouqu, Gansu Province, China, caused 1434 casualties with a further 331 people reported missing (Tang et al. 2011). Risk assessment can provide strong technical support for implementing policies for disaster prevention and reduction. Thus, risk assessment of debris flows is extremely important for protecting life and property, for disaster prevention and mitigation, and for carrying out risk management and ecological restoration.

Based on the definition provided by the United Nations, risk is a measure of the loss of life, personal injury, loss of property, and disruption of economic activity caused by

specific hazards in specific areas and during reference periods and is represented by a value between 0 (0%) and 1 (100%) (United Nations 1991). Risk has three fundamental components: hazard, elements at risk or exposure, and vulnerability (Liu and Lei 2003; Eidsvig et al. 2014; Himmelsbach et al. 2015). Considerable contributions have been made to assess debris flow risks (Takahashi et al. 1992; Hurlimann et al. 2006; Armanini et al. 2009; Magirl et al. 2010; Iverson et al. 2011; Liang et al. 2012; Berti and Simoni 2014; Iverson and Ouyang 2015; Chen et al. 2015a; Chen et al. 2016; Wang et al. 2016; Gao et al. 2016; Kang and Lee 2018; Wei et al. 2018). A comprehensive analysis found that the current researches generally use the two methods (statistical analysis and numerical simulation) to carry out debris flow risk analysis.

Statistical analysis method According to the definition of risk, it can be mathematically translated as a product of hazard and vulnerability mathematically (Liu and Lei 2003). Therefore, based on the quantitative analyses of hazard and vulnerability using relevant factors, debris flow risk can be determined by superimposing the results of hazard and vulnerability. The hazard analysis of debris flow based on this method generally selects factors that are closely related to the formation of debris flows (e.g., frequency, magnitude, slope, length of main channel, watershed area, etc.) to indirectly evaluate the hazard (Wang et al. 2016). Thirteen indicators (i.e., slope, aspect, curvature, soil thickness, soil drainage, soil texture, soil material, soil topography, timber type, timber age, timber density, timber diameter, and land cove) were selected to assess the degree of hazard of debris flows in Korea by Jinsoo et al. (2013). Wang et al. (2014) selected the watershed area, length of main channel, elevation difference, and loose solid material reserve as indicators to evaluate the debris flow hazard in Shenxi watershed, Sichuan Province, China. The debris flow vulnerability analysis based on the statistical analysis method generally establishes quantitative relationships between debris flow vulnerability and the economy, society, and population factors (Fuchs et al. 2007; Akbas et al. 2009; Lo et al. 2012; Totschnig and Fuchs 2013). For instance, Cutter et al. (2003) employed a factor analysis approach and 11 independent factors to compute the social vulnerability index for the United States. Hu et al. (2016) presented a matrix classification scheme to evaluate building damage for brick and reinforced concrete structures. An improvement of the vulnerability curve as a function of process intensity and loss extent is presented using the debris flow events data in South Tyrol (Papathoma-Köhle et al. 2012). Based on the information from hazard and vulnerability assessments, the debris flow risk can be evaluated by superimposing the results of hazard and vulnerability. Comprehensively, the above statistical analysis method must provide information that can replace the empirical data necessary for debris flow risk derivation. Moreover, they cannot elucidate the dynamic inundation

process or the interactions between the disaster and the elements at risk. Therefore, statistical methods are only applicable to large-scale regional risk analysis, and not to the dynamic risk analysis of a disaster event.

Numerical simulation method As for this method, this risk analysis method is also based on initial separate assessments of debris flow hazard and vulnerability; however, they are combined for the final risk analysis. This method cannot only provide dynamic information about key inundation parameters (such as flow velocity, depth, and inundated area) but can also reflect the interactions between the flow and the elements at risk. Therefore, many researchers have been devoted to this issue since the 1990s (O'Brien et al. 1993; Hungr 1995; Sousa and Voight 1995; Chen and Lee 2000; Romenski and Toro 2004; Spence et al. 2004; Totschnig et al. 2011; Luna et al. 2012; Kwan et al. 2013; Pudasaini 2016; Bout et al. 2018). For instance, Fuchs et al. (2007) established the relationship between debris flow depth and building vulnerability, with particular emphasis on building materials. Liu et al. (2009) used the empirical formulae for estimating the expected loss of the land use under different recurrence intervals according to the simulated results of Debris-2D software. Jakob et al. (2012) proposed an index (IDF) to determine building vulnerability, which was expressed by the product of the maximum expected flow depth (d) and the square of the maximum flow velocity (v) ($IDF = dv^2$). Zhang et al. (2018) proposed a series of debris flow vulnerability models to evaluate the building damage caused by a debris flow event. Currently, with improvements in disaster mechanism models and computer technology, considerable progress has been made in research on risk analysis of debris flow based on the numerical simulation method. However, the evaluation of debris flow vulnerability specifies neither the kinetics or process intensity characteristics, nor the physical mechanisms or the property of land uses. In particular, the relationship between process intensity information and the property of land uses is not yet well understood. Moreover, although considerable disasters have occurred in recent years, no sound quantitative relationship has been established between debris flow risks and land uses.

The overall purpose of this study was to propose and test a methodology for the debris flow risk assessment by incorporating numerical simulations with different land use types. The specific objectives were as follows: (i) propose a debris flow hazard classification model on the basis of a combination of the debris flow intensity and the return periods to map debris flow hazard, (ii) establish a simplified method to quantify the vulnerability of different land use by evaluating the degree of functional damage under the given hazard level intensity, (iii) produce a debris flow risk zone by combining debris flow hazard and vulnerability, and (iv) conduct a case study and test the proposed methodology. To achieve these objectives, a small debris flow gully was selected as the case study site for the application of the proposed methodology.

Materials and methodology

The methodology for the proposed debris flow risk analysis and modeling can be divided into four steps (Fig. 1): (i) data classification and data processing, (ii) numerical simulation and hazard assessment for different return periods, (iii) land use determination within the debris flow inundated area, and (iv) vulnerability and risk assessment of debris flows.

Data classification and data processing

The accuracy of risk assessment of debris flow disaster is highly dependent on basic data such as geology, topography, lithology, rainfall, hydrology, soil, vegetation, and human activity. Here, these basic data are classified into four categories based on the topographic, material, hydrology, and management data. Topographic data are mainly fine digital terrain maps, such as the digital elevation model (DEM), and used to provide basic terrain information affecting the accuracy of debris flow simulation. Material data describes the attribute of the loose solid material and debris flow in the field, including key physical and mechanical parameters (such as particle density, fluid average density, and rheology or friction types) and is used to identify the material and flow properties for numerical simulations. Hydrological data includes rainfall and field monitoring data of water level over previous years, intensity–duration–frequency curves, and hydrological records of previous important events, which are used to provide inflow parameters for debris flow simulations. Management data mainly include remote sensing image data, historical disaster events and disaster loss data, on-site investigation data, land
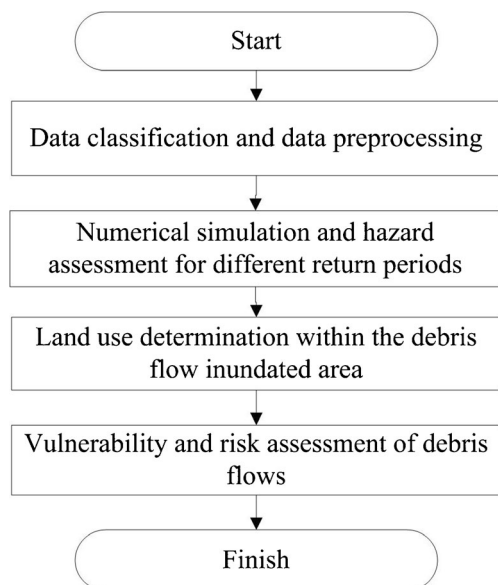

Fig. 1 Block diagram of procedure for debris flow risk assessment proposed in this article

utilization data, and social and economic data, which are generally used for debris flow risk assessment and mapping. After classification, the above data were rectified and georeferenced to the uniform reference coordinate system.

Numerical simulation and hazard evaluation for different return periods

Debris flow numerical simulation for different return periods

Rainfall under different return periods can trigger different magnitudes of debris flow events (Liu et al. 2009). To conduct detailed debris flow risk assessments, the relevant parameters corresponding to different return periods (such as flow depth, flow velocity, and inundated area) should be identified first. In this study, the numerical method was used to obtain the relevant key debris flow parameters of debris flow risk assessment.

The model can be applied for modeling mountain hazards (such as dam break, landslide, and debris flow) with a MacCormack-TVD finite-difference code (Ouyang et al. 2015a, 2015b). This model generates a detailed computational mesh by defining the mesh type, the number of mesh cell, and the node coordinates. The boundary condition contains the symmetrical boundary, open boundary, wall boundary, etc., which can be input by system-provided and user self-programming. The necessary parameters for computation are a digital topographical map (DEM), material attribute data of fluent and river bed, flow height or volume, and the outlet of the debris flow. The digital topographical map is used to create the initial depth of the motion and must be sufficiently detailed to obtain accurate results. Attribute data contains basic physical parameters of the loose material and flow (such as particle density, water density, fluid average density, cohesion, internal friction angle, flow density, etc.) and friction behavior type of debris flow (Coulomb, Manning; Voellmy; Bingham and custom friction types are provided), to serve as the initial input necessary parameters, which can be measured by conducting outdoor and indoor tests on field samples. Initial inflow conditions (such as flow velocity, flow height, and volume) are generally input through user self-programming. The outlet of the debris flow initial motion can be derived from field surveys combined with the aerial photos. The volume of mobilized debris flow under different return periods can be obtained as follows.

The debris flow concentration is used here and is calculated by the equilibrium concentration equation (Takahashi 1980), which is shown as:

$$C_{d\infty} = \frac{\rho \tan\theta}{(\sigma - \rho)(\tan\phi - \tan\theta)}, \tag{1}$$

where $C_{d\infty}$ is the equilibrium concentration of the debris flow; ρ is the density of the fluid in the debris flow (for water,

fluid density is 1.0 g/cm^3; for clayey water, fluid density is 1.2 g/cm^3); θ is the average slope of the riverbed (°) and can be obtained through statistics on topographic data; σ is the density of the solid particles, which is usually 2.65 g/cm^3; and ϕ is the angle of friction of the solid particles (°), which is obtained from laboratory experiments of direct shear tests or triaxial compression tests.

The amount of mobilized material in the field is determined based on the amounts of precipitation and debris sources (Chen et al. 2015b). If the amount of precipitation is relatively small, only a small part of the loose material on the slope or river bed can be mobilized to form a debris flow. As the amount of precipitation increases, so does the amount of the mobilized material until all the material is eroded. However, if the amount of precipitation is greater than the amount of loose material required to form a debris flow, a mixture of water with the debris flow occurs. Therefore, the debris flow volume should be determined by the amount of loose materials on the riverbed or hill slope and the amount of local precipitation, which can be calculated as Liu et al. (2009):

$$V_D = \min\left\{\frac{V_s}{C_{d\infty}}, \frac{V_w}{1-C_{d\infty}}\right\}. \tag{2}$$

where V_s is the available field debris source volume on the riverbed or hill slope (m^3), V_w is the amount of precipitation during the rainfall event in a debris flow watershed (m^3), $C_{d\infty}$ is the equilibrium concentration of the debris flow, and V_D is the debris flow volume induced by the precipitation (m^3).

In practice, the available field debris source volume (V_s) is generally determined by intensive field investigations combined with aerial photos. The precipitation amount (V_w) for different return periods, as well as other key design parameters, such as the 10 min, 1 h, 6 h, and 24 h rainfall intensity, and the maximum flood peak discharge, can be obtained from the Sichuan Hydrology Record manual (Shen et al. 1984). With the above parameters, the total volume of debris flow (V_D) for different return periods can be calculated using Eqs. 1 and 2.

After preparing the necessary parameters for numerical simulation of this model including boundary condition, initial condition, material attribute data, and mesh generation, the debris flow movement velocities, maximum flow depths, intensities, and inundated areas for different return periods can be simulated. Figure 2 shows a typical simulation based on the model.

Debris flow hazard assessment for different return periods

Hazard assessment of debris flows was conducted based on three simulations, using as input rainfall with 20-, 100-, and 200-year return periods, respectively. According to Swiss and Austrian standards (Fiebiger 1997), the yearly occurrence

probability of debris flows based on the corresponding return period can be obtained as:

$$P_n = 1-\left(1-\frac{1}{T}\right)^n, \tag{3}$$

where P represents the yearly occurrence probability of debris flow based on the corresponding return period. T is the debris flow recurrence period, and the value of n is 1 for a yearly probability. According to the Taiwan Debris Flow Risk Classification (Lin et al. 2011), the following classification is adopted for the probability of an outbreak of a debris flow: more than 5% high probability; between 5 and 1%, moderate probability; low probability, between 1 and 0.5%; and very low probability, less than 0.5% (O'Brien 2004; Chang et al. 2017). The precipitation amounts (V_w) for the 20-, 100-, and 200-year return periods were obtained by the Sichuan Hydrology Record manual (Shen et al. 1984). The total volume of debris flow (V_D) for the 20-, 100-, and 200-year return periods were calculated using Eqs. 1 and 2.

Based on the Swiss and Austrian standards (Fiebiger 1997) and the Taiwan Debris Flow Risk Classification (Lin et al. 2011), the debris flow intensity and probability of occurrence were used in this article to create a debris flow hazard map. In the researches, such as Giuseppe et al. (2012), Regione Sicilia (2004), and Chang et al. (2017), the return period and the intensity were also combined to determine the debris flow hazard. The debris flow intensity is defined as the maximum simulated depth (h) multiplied by the maximum simulated velocity (v) and the maximum simulation depth (h). Table 1 shows the classification of the intensity based the hv and h proposed by Lin et al. (2011) and Chang et al. (2017). Combining the intensity classes with the occurrence probability classes, calculated according to Eq. 3, three hazard classes were adopted in this study (Fig. 3). Based on this classification, a hazard map for the study can be obtained.

The above hazard classification of debris flow is related to the intensity and occurrence probability, which can be classified into three categories (Fig. 3): (i) high hazard (H_3) causing severe structural damage corresponds to conditions under high intensity and high probability, high intensity and moderate probability, or moderate intensity and high probability; (ii) moderate hazard (H_2) causing weak structural damage depending on its specific property corresponds to conditions of high intensity and low probability, moderate intensity and probability, or high probability and low intensity, and elements may suffer weak structural damages depending on the specific property; and (iii) low hazard (H_1) is a minimum flooding situation, which refers to moderate intensity and low probability, low intensity and moderate probability, or low intensity and low probability. It is observed that the hazard of debris flow varies with the occurrence probability and intensity. Larger-scale events occur less frequently but have

Fig. 2 A typical numerical simulation result for a debris flow event. The debris flow inundated area and buried depth are shown in the figure. Different colors indicate depths of the debris flow (Wang et al. 2016)
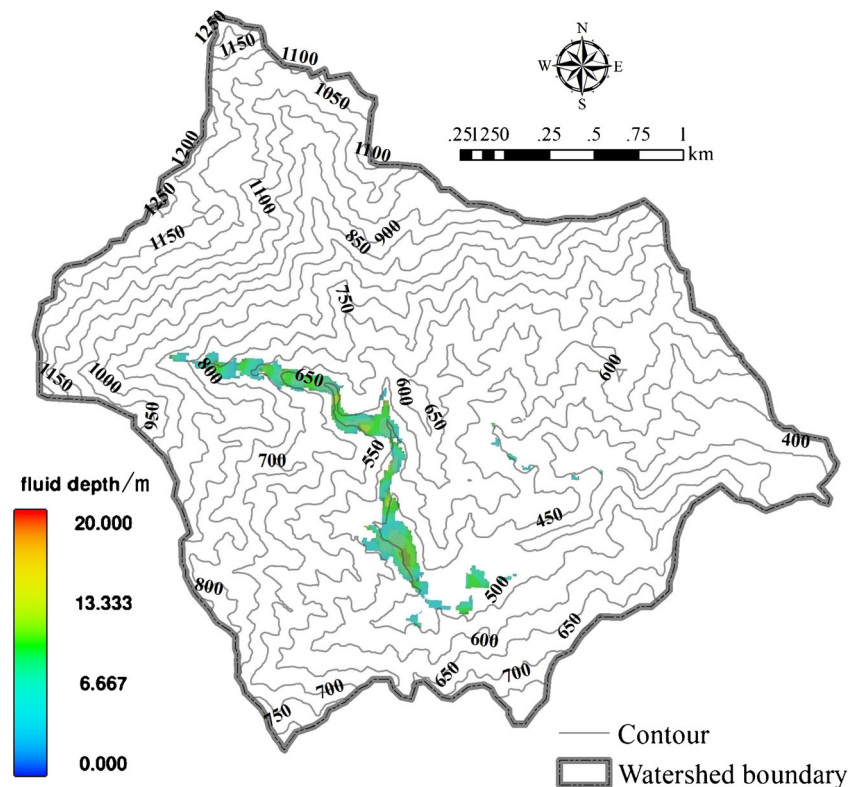
higher intensity expressed in terms of flow depth and velocity. Smaller-scale events are more frequent but have smaller intensity. The methodology to delineate debris flow hazard map used in this study was first applied in northern Venezuela, and it is based on Swiss and Austrian standards (Gentile et al. 2008; Lin et al. 2011; Chang et al. 2017). Three zones of different hazard levels are defined (Fig. 3). The occurrence probability is defined for return periods of 20, 100 and 200 years; the intensity depends on the combination of flow depth (h) and flow velocity (v).

Land use determination within debris flow inundated areas

According to the numerical simulated results of debris flows under different rainfall periods, the land use types within the inundated area can be determined. Here, the current land use classification standard issued by the Standardization Administration of the People's Republic of China was used

to classify the land use types in this article (PRC National Standard GB/T 21010-2017). The 12 first-class land use classes, namely, cultivated land, garden land, forest, grassland, commercial land, industrial and mining storage land, residential land, public management and public service land, special land, transportation land, water/water conservancy facilities, and other land, were classified (Table 2). In practice, based on Landsat TM digital images combined with the above land use classification standard, the spatial distribution of land use can be mapped by employing the full digital interactive remote sensing extraction method. Then, the land use within the inundated area can be extracted from the inundated area boundary based on the numerical simulation results.
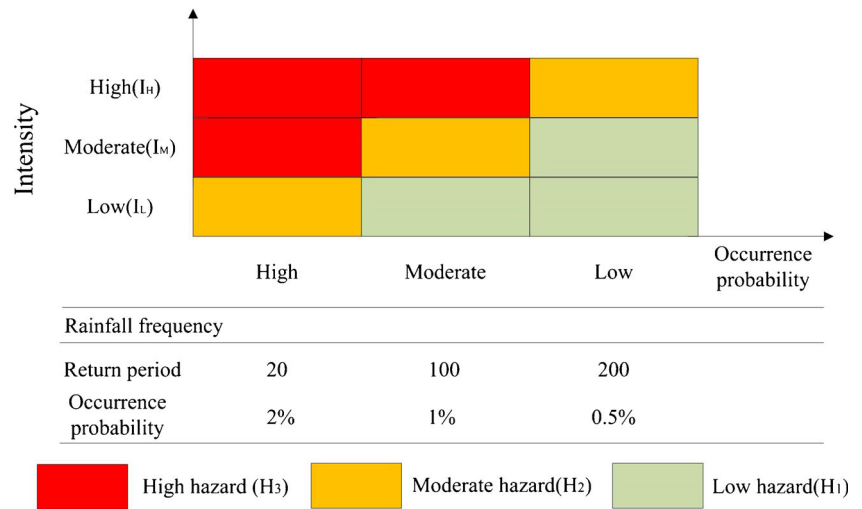
Vulnerability and risk assessment of debris flow

Risk is defined as the expected loss of life, personal injuries, property damage, and economic activity disruption due to a particular natural phenomenon. Mathematically, it can be

Table 1 Debris flow intensity divided standard used in this study

Debris flow intensity	Maximum simulated accumulation depth h (m)	Relation	Maximum simulated accumulation depth and velocity vh (m²/s)
High (I_H)	$h \geq 2.5$	Or	$vh \geq 2.5$
Moderate (I_M)	$0.5 \leq h < 2.5$	And	$0.5 \leq vh < 2.5$
Low (I_L)	$0.0 \leq h < 0.5$	And	$0.0 \leq vh < 0.5$

Fig. 3 Classification of the degree of hazard for debris flows proposed in this study

Rainfall frequency			
Return period	20	100	200
Occurrence probability	2%	1%	0.5%

High hazard (H3)   Moderate hazard(H2)   Low hazard(H1)

translated as the product of hazard and vulnerability (Eidsvig et al. 2014):

$$R = H{\cdot}V, \qquad (4)$$

where hazard (H) is the physical property of a disaster itself (as discussed in detail in the "Debris flow hazard assessment for different return periods" section) and vulnerability (V) refers to the extent of loss to the element at risks under a given debris flow intensity and ranges between 0 (no loss) and 1 (total loss). Here, the element at risks refers to the land use within the inundated areas. Risk includes both the probability of debris flows occurrence and element losses.

Vulnerability is determined by the hazard of debris flows and the property of the elements at risk (land uses). The vulnerability assessment is complicated by the problem of having

to assume a specific monetary value and the difficulty of assessing the physical, social, and economic capacity of people to react to the disaster occurrence. Followed by Fuchs et al. (2007), a simplified method able to quantify the vulnerability is proposed by dividing the elements at risk (land uses) into several classes (12 first-class land use classes, seen as Table 2) and then using an indicator of functional damage degree or the cost of recovery to the land use derived from the occurrence of a debris flow event under a given intensity. The final vulnerability can be classified into three distinct classes: (i) low vulnerability ($V_1 < 0.3$), superficial (minor) damage, where the elements at risk are functionally unimpaired and can be easily and quickly restored; (ii) moderate vulnerability ($0.3 \leq V_2 < 0.6$), functional (moderate) damage, where the function of the elements at risk is impaired, and the recovery of the element requires considerable time and cost; and (iii) high

Table 2 The land use type classification standard used in this article

Land use law	Land use types	Content
E1	Cultivated land	Paddy field, irrigated fields, dry land, etc.
E2	Garden land	Fruit land, tea land, betel field, etc.
E3	Forest use	Broadleaf wood, coniferous wood, bush woods, bamboo field, etc.
E4	Grassland	Natural pasture land, artificial pasture land, etc.
E5	Commercial land	Wholesale and retail land, accommodation and catering land, commercial and financial land, etc.
E6	Industrial and mining storage land	Industrial land, mining land, storage field, etc.
E7	Residential land	Urban residential land and rural residential land
E8	Public management and service land	Scientific education land, medical treatment land, sports and entertainment land, press and publication land, public facilities and scenic spots l and, park and green spaces field, etc.
E9	Special land	Military installations, religious sites, funeral sites, etc.
E10	Transportation land	Railway, highway, rural road, airport, port and dock land, pipeline transportation, etc.
E11	Water and water conservancy facilities	River, lake, reservoir, fish pond, tidal flats, ditches, hydraulic structures, etc.
E12	Other land use	Salt and alkaline land, swamp land, sand, bare land, etc.

vulnerability ($0.6 \leq V_3 < 1.0$), structural (total) damage, where the elements at risk are severely or completely damaged and the function of the element cannot be recovered. In this regard, demolition and reconstruction may be carried out. According to the special attribution of land uses, the vulnerability of 12 first-class land use classes can be determined, followed by the suggested standard for seven different types of land utilization proposed by Liu et al. (2009), which is shown in Table 3.

The debris flow risk assessment result is generated by overlaying the hazard and vulnerability results. The product is a debris flow risk map in which high (R_3), moderate (R_2), and low (R_1) risk areas are identified (Fig. 4 and Table 3). Figure 4 shows the risk matrix composed of hazard and vulnerability. Table 3 shows that the qualitative division of the risk is divided into three classes based on hazard and vulnerability of debris flows. In general, the maximum loss of a disaster is considered when conducting risk assessment. Therefore, the above risk classification method based on the maximum risks of land uses for different purposes is reasonable when conducting disaster prevention and mitigation.

The case study

Study area description

A debris flow gully located in Southwest China was chosen as the study site (Fig. 5). The watershed area is approximately 8.63 km^2 with a maximum elevation of approximately 2492 m, and the length of main channel is nearly 4.4 km. The river gully gradient is relatively large, ranging from 0° to 64°. The typical channel slope range is between 30 and 40°, accounting for 48.69% of the study area. The basic characteristic parameters of the debris flow gully watershed are listed in Table 4.

The area has a subtropical monsoon climate, where rainfall is seasonal with average annual rainfall of approximately 1200 mm/year. Rainfall events are characterized by short concentration times and hydrological responses. The Wenchuan earthquake on May 12, 2008, produced a considerable amount of unstable loose material in the watershed. Ma et al. (2011) estimated that the loose material reserve induced by the Wenchuan earthquake was more than 757.61×10^4 m^3 which could be easily mobilized to form debris flows. Consequently, this area represents a high-damage-risk area under the combined action of the meteorological and geological–morphological conditions, as confirmed by the debris flow event on August 13, 2013.

Application of the proposed methodology and results

The basic data used in case study were topographic data, material data, hydrology data, and management data. The

Table 3 Risk classes used in this article

Hazard	Exposure E1 Vulnerability	Risk	E2 Vulnerability	Risk	E3 Vulnerability	Risk	E4 Vulnerability	Risk	E5 Vulnerability	Risk	E6 Vulnerability	Risk
H1	Superficial (minor) damage	Low	Superficial (minor) damage	Low	Superficial (minor) damage	Low	Superficial (minor) damage	Low	Functional (moderate) damage	Low	Functional (moderate) damage	Low
H2	Functional (moderate) damage	Moderate	Functional (moderate) damage	Moderate	Superficial (minor) damage	Moderate	Superficial (minor) damage	Low	Structural (total) damage	High	Structural (total) damage	High
H3	Structural (total) damage	High	Structural (total) damage	High	Superficial (minor) damage	High	Superficial (minor) damage	Moderate	Structural (total) damage	High	Structural (total) damage	High

Hazard	Exposure E7 Vulnerability	Risk	E8 Vulnerability	Risk	E9 Vulnerability	Risk	E10 Vulnerability	Risk	E11 Vulnerability	Risk	E12 Vulnerability	Risk
H1	Superficial (minor) damage	Low	Superficial (minor) damage	Low	Functional (moderate) damage	Low	Functional (moderate) damage	Moderate	Superficial (minor) damage	Low	Superficial (minor) damage	Low
H2	Functional (moderate) damage	Moderate	Functional (moderate) damage	Moderate	Structural (total) damage	Moderate	Structural (total) damage	High	Functional (moderate) damage	Moderate	Superficial (minor) damage	Low
H3	Structural (total) damage	High	Structural (total) damage	High	Structural (total) damage	High	Structural (total) damage	High	Structural (total) damage	High	Superficial (minor) damage	Moderate

Fig. 4 The risk matrix used in the study
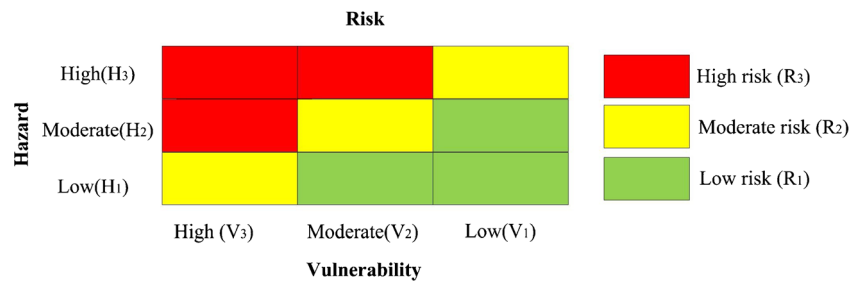
topographic data was the DEM with 5-m resolution. The material data were mainly the attributes of the material (derived from in/outdoor tests of soil samples of debris flow source area) and the debris flow (derived from in/outdoor tests of soil samples of debris flow accumulation area). The hydrology data mainly consisted of rainfall data obtained over the past 20 years; the historical statistics of 10 min, 1 h, daily, monthly, and yearly rainfall; and the rainfall records corresponding to important previous disasters. The management data were mainly remote sensing images including the multi-period Landsat 8 satellite images and Google Earth images, the details of previous disasters, the results of intensive on-site investigations, and section measurement data. The land use types in the study are obtained as follows: according to

the current land use classification standard (PRC National Standard GB/T 21010-2017), the Landsat-8 remote sensing image of the study area was used as the data source to classify the initial land use types by the supervised classification method of the ENVI software. Then, the field survey method was used to verify the accuracy of the initial results of supervised classification. The land use final classification map of the study area can be obtained after verification.

According to the Sichuan Hydrology Record manual (Shen et al. 1984), the relevant key design parameters of the drainage outlet, such as the 10 min, 1 h, 6 h, and 24 h rainfall intensity, and the maximum flood peak discharge can be obtained, as can be seen in Table 5.
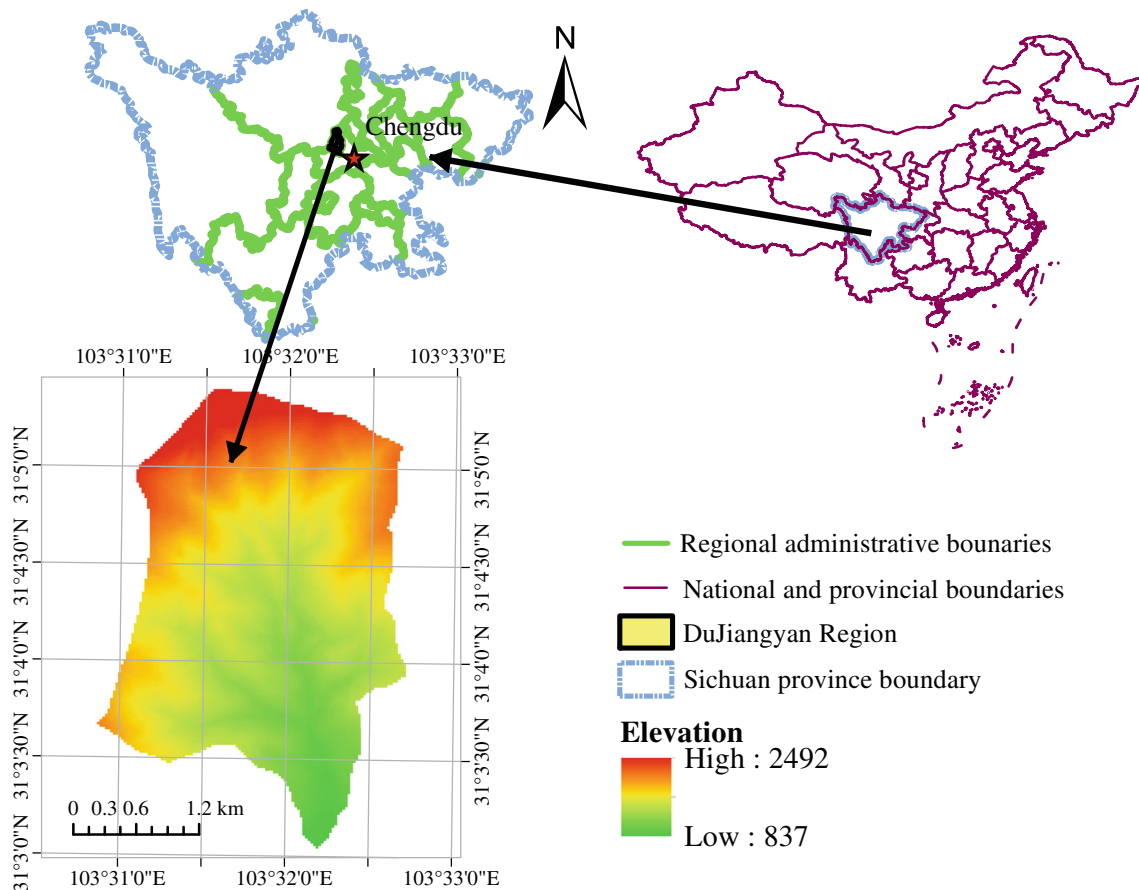

Fig. 5 The location of the study area

Table 4 Morphological characteristics of the study area

Morphological factors	Value
Area (km^2)	8.63
Max altitude (m a.s.l.)	2492
Elevation difference (km)	1.65
Main river channel length (km)	4.45
Average channel slope (m/m)	0.37
Range	31° 03′ 01″ ~ 31° 05′ 22″ N; 103° 30′ 57″ ~ 103° 32′ 41″ E

The equilibrium concentration of a debris flow can be calculated using Eq. 4. The values of the parameters in Eq. 4 derived from the material data are as follows: $\rho = 1000$ kg/m^3, $\varphi = 38°$, $\sigma = 2450$ kg/m^3, and $\theta = 22.34°$. The equilibrium concentration was calculated as:

$$C_d = \frac{\rho \tan\theta}{(\sigma-\rho)(\tan\varphi-\tan\theta)} = \frac{1000 \times 0.411}{1450 \times 0.370} \cong 0.76 \qquad (5)$$

The different volumes of debris flow for the corresponding return periods were calculated using Eq. 6 and are summarized in Table 5. According to our field surveys as well as related research of Ma et al. (2011), more than 600×10^4 m^3 of the loose material remains on the hill and in the main channel, which would be mobilized to form debris flows induced by heavy rainfall. Thus, the total volume of available material (V_s) was set to 600×10^4 m^3. With sufficient precipitation, all of the debris materials can be mobilized. The maximum debris flow volume was:

$$V_D = \min\left\{\frac{V_s}{C_d}, \frac{V_w}{1-C_d}\right\} = \frac{600}{0.76} \times 10^4 (m^3) \cong 783 \times 10^4 (m^3) \quad (6)$$

The rainfall event which occurred on August 13, 2013, had a return period of approximately 100 years and triggered a large-scale debris flow rushing out about 116×10^4 m^3 of loose solid materials (Ma et al. 2011). We used the research results presented by Ma et al. (2011) to validate our calculated results in Table 5 with the same return period of 100 years and found that the calculated result value was close to the field survey result of Ma et al. (2011).

Table 5 The key design parameters for 20-, 100-, and 200-year return periods

Return period/year	20	100	200
10-min rainfall intensity/mm	20.76	26.76	29.16
1-h rainfall intensity/mm	82.68	111.8	121.68
6-h rainfall intensity/mm	197.00	269.00	300.00
24-h rainfall intensity/mm	318.08	467.18	531.08
Debris flow volume/ $\times 10^4$ m^3	42.00	115.50	349.50

Therefore, the calculated flow volumes presented in Table 5 are reasonable for the debris flow simulation with different return periods.

Generally, the outlet of debris flows was determined by field investigations and the interpretation of remote sensing data. The outlet of the debris flow used for numerical simulation under different return periods in this study is shown in Fig. 6. The catchment area and length above this outlet are 4.28 km^2 and 3.1 km, respectively. On-site investigations were conducted to determine the debris flow density. The mean of multiple measurements of typical deposits of the debris flow event on August 13, 2013, was chosen as the flow density for the numerical simulations with different return periods. The material rheological parameter was measured using an MCR301 rheometer in the laboratory. The debris flow was determined to be a Voellmy model based on rheological testing of the slurry. The basic input parameters are shown in Table 6. The topographic boundary condition for debris flow simulation was derived from high-resolution DEM (5×5 m). The bed erosion was not considered in this study and the boundary conditions were set by default, i.e., wall boundary conditions. The outlet was set as the inflow boundary condition for the flow volume corresponding to different rainfall periods. The flow height was controlled by the debris flow volume and the topography of the input outlet. After preparing all the necessary parameters and boundary conditions, the mesh type, the number of mesh cell, and the node coordinates were defined to conduct debris flow simulation.

The numerical simulation results for the maximum flow depths for 20-, 100-, and 200-year return periods are shown in Fig. 7. The fluid motion parameters have a high degree of uncertainty and the following method was used to verify the accuracy of the numerical simulation.
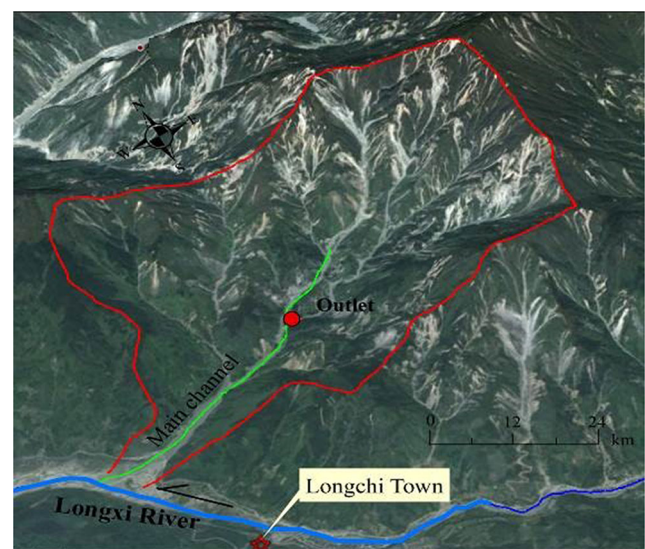

Fig. 6 The location of the out and gully condition in the study area

Table 6 The input parameters of flow in the proposed model

Particle density ρ_s/kg/m³	Water density ρ_w/kg/m³	Average flow density $\bar{\rho}$ /kg/m³	Internal friction angle ϕ/°	Bed friction angle δ/°	Internal friction angle of the flowing mass $\phi_{Voellmy}$/°	Chezy coefficient	Pore pressure ratio
2450	1000	1850	40	40	12	12	0.8

The observed parameters ($A_{observed}$) of the selected debris flow events were based on field surveys. The predicted parameters ($A_{predicted}$) were defined as the debris flow motion parameters simulated by the numerical model. The evaluation parameter (relative error Ω, a value indicating the overall accuracy of the simulated events) can then be calculated as:

$$\Omega = \frac{A_{predicted} - A_{observed}}{A_{observed}} \times 100\% \tag{7}$$

The rainfall on August 13, 2013, had a 100-year return period. After the event, we conducted numerous field investigations and measurements and measured the inundated area, damaged houses, casualties, and damage to different land use types. Therefore, this debris flow disaster event was used to verify the debris flow simulation. We selected the fluid depth and the inundated area as the validated parameters. The result of the field investigation of flow depth for a building house on the debris flow fan was approximately 6.0 m, and the numerical simulation result was 7.075 m, yielding an error of 17.9% ($\Omega = 17.9\%$). The simulated result of the inundated area was approximately 9.55×10^3 m², with a relative error of 21.1%

($\Omega = 21.1\%$). Therefore, the numerical simulation results under a 100-year return period are in agreement with the field surveys. Hence, the proposed method can be used to simulate debris flow inundated parameters and to calculate debris flow intensities.

After obtaining the key parameters of debris flow for different return periods (such as the influence area, flow depth, and flow velocity), a final debris flow hazard map can be obtained by using the proposed hazard assessment standard of debris flows (Figure 3), as shown in Fig. 8.

The land use properties of the study area within the maximum influence area corresponding to the 200-year return period are mainly cultivated land (E1), forestland (E3), grassland (E4), residential land (E7), transportation land (E10), rivers (E11), and bare land (debris flow deposit area, E12), as shown in Fig. 9. These land uses were artificially mapped through intensive fieldwork combined with remote sensing images.

Vulnerability is determined by the hazard of debris flows and the properties of land uses (Table 3). The water land (E11) is mainly the Longxi River and Dagangou River, which are important sources of water for the Zipingpu reservoir
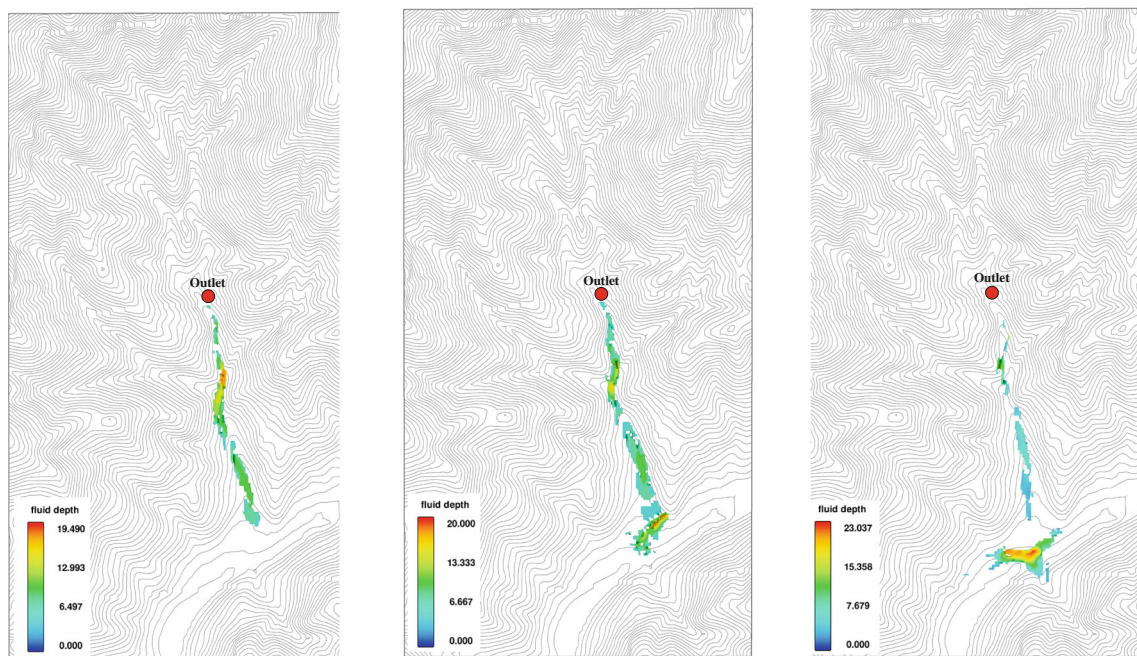

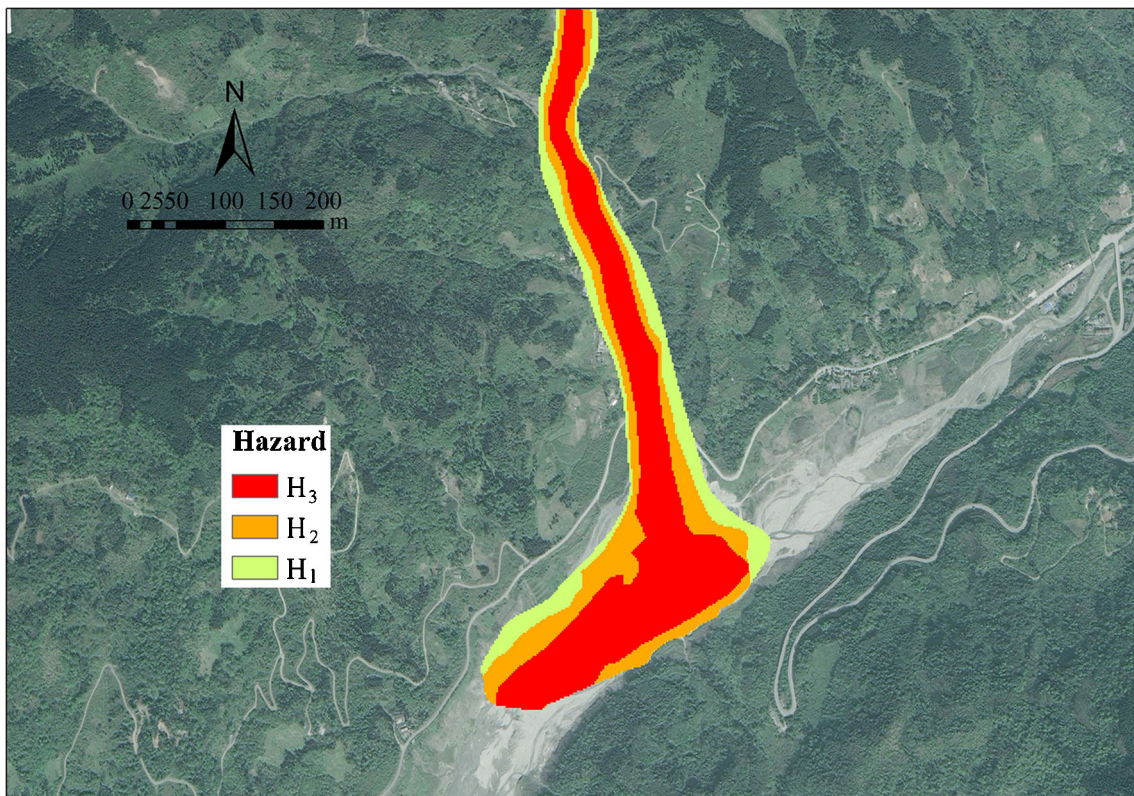**Fig. 7** Numerical simulation results of final buried depths under rainfalls with different return periods
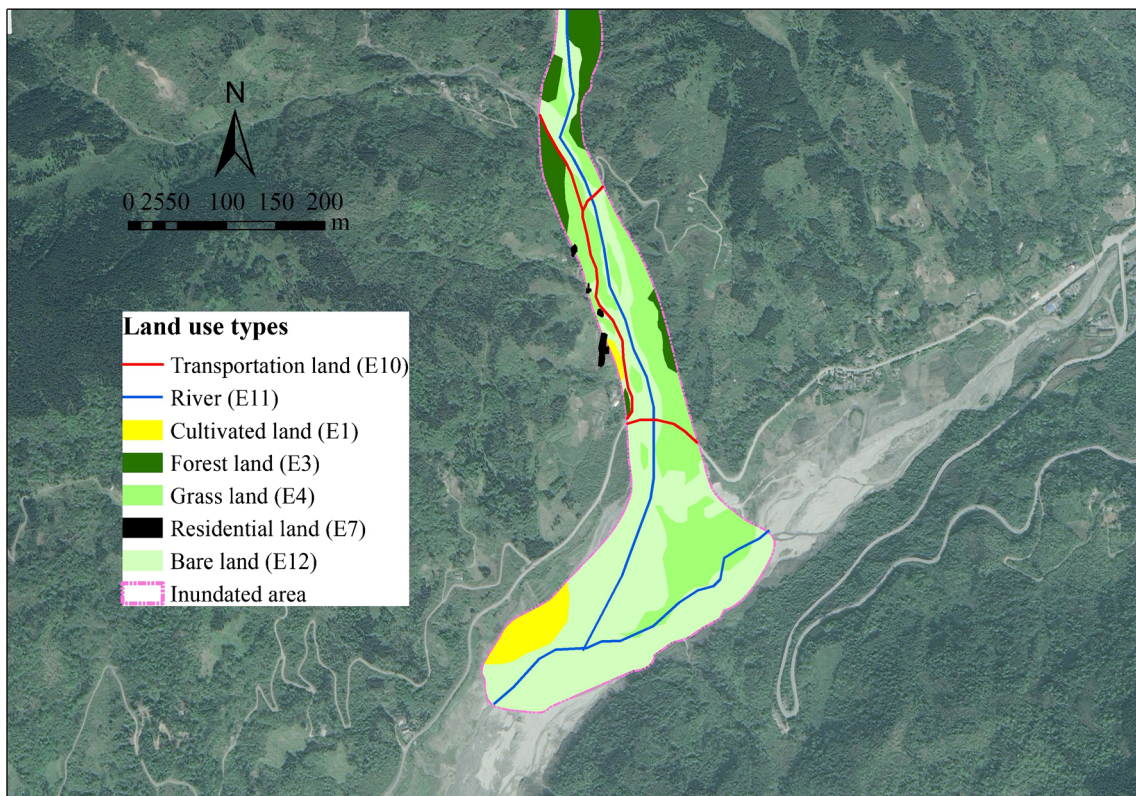
Fig. 8 Hazard map

Fig. 9 Land use types within the influenced area

providing drinking water for Dujiangyan City, China. Thus, it is considered a high-risk level. The other land in this area (E12) is mainly a debris flow deposit area and is considered a low-risk area. The other land use risks are determined by the risk matrix (Table 3). Based on them, the debris flow risk map was finally generated (Fig. 10), which shows the risk qualitatively classified into three classes (low, medium, and high). Figure 10 also shows that residential land and transportation land show a high risk. Moderate risk is distributed in cultivated land, grassland, and forestland. Low risk is mainly distributed in cultivated land, forestland, and bare land.

Discussion

In this study, the roughly 12 first-class land use class vulnerabilities under different hazard intensities were assessed. However, each first-level land use type contains multiple second-level types. For example, the transportation land use type contains railway, highway, rural road, airport, port and dock land, pipeline transportation, etc. Under the same hazard level, the vulnerability of different secondary-class land use types is also different. The deficiency of this study is that it did not consider the different vulnerabilities of secondary-class land use indicators. However, this study considered the

maximum value of the vulnerability of the second-class land use indicators and used this value as the vulnerability of each first-class land use types. In the following research, the vulnerability assessment methods and models for secondary-class land use types will be conducted, making the vulnerability assessment of debris flow more reasonable and better applied to the practice of debris flow disaster prevention and mitigation.

Conclusions

In this study, the debris flow risk analysis and modeling were performed by combining numerical simulations with land utilization data and the proposed methodology was tested by a case study area of a small catchment. The main conclusions are the following:

(1) The debris flow process intensity and the probability of occurrence were used to create a debris flow hazard map. The debris flow intensity was defined as the product of maximum simulated depth (h) and fluent velocity (v) or the maximum simulated depth (h). Joint with the 20-, 100-, and 200-year return periods, three hazard classes (high, moderate, and low) were adopted, indicative of the
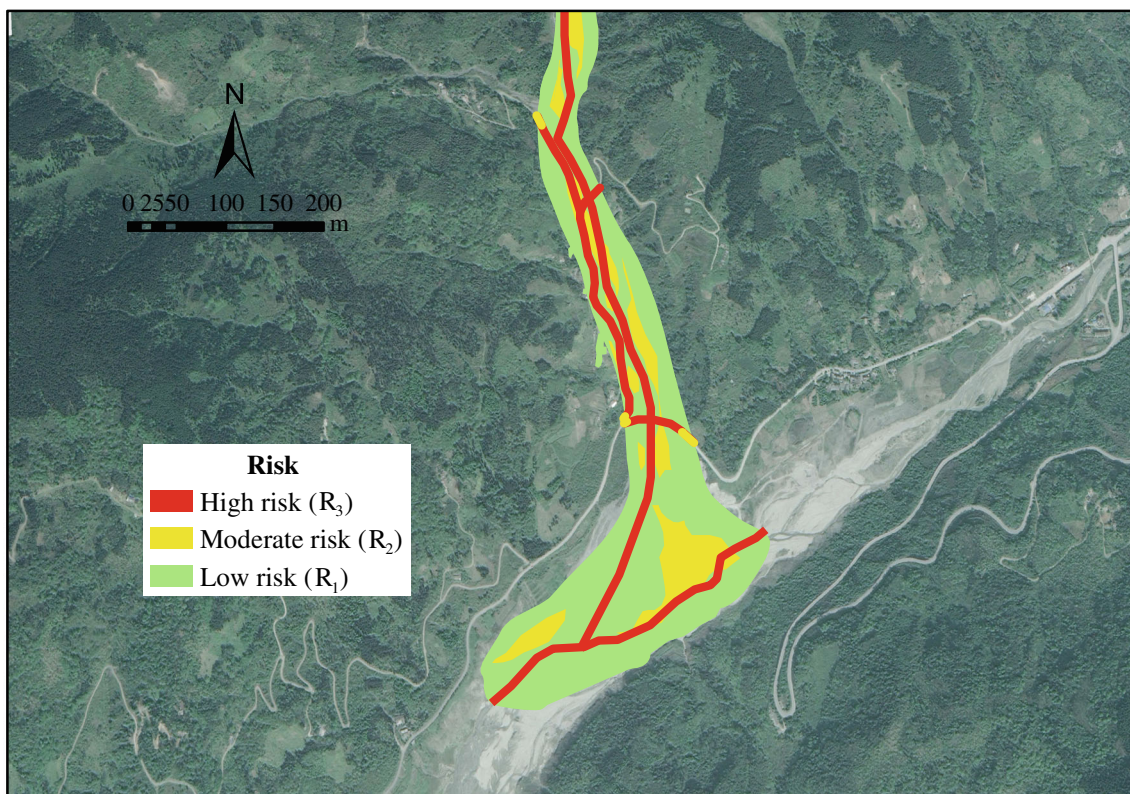

Fig. 10 Risk map

potential level of damage to land uses within the inundated areas.

(2) A simplified method able to quantify the vulnerability of 12 first-class land use classes by evaluating the degree of functional damage under the given hazard class was put forward. Each land use type has three vulnerability categories: superficial damage (low vulnerability), functional damage (moderate vulnerability), and structural damage (high vulnerability).

(3) After the hazard and vulnerability assessments of debris flows, the final debris flow risk assessment was conducted by combining the hazard and vulnerability assessment results. The final risks were classified into high (R_3), moderate (R_2) and low risk (R_1).

References

Akbas SO, Blahu J, Sterlacchin IS (2009) Critical assessment of existing physical vulnerability estimation approaches for debris flow [J]. In: Malet J, Remaitre A, Bofaard T (eds) Landslide processes: from geomorphological mapping to dynamic modeling. CERG Editions, Strasbourg, pp 229–233

Armanini A, Fraccarollo L, Rosatti G (2009) Two-dimensional simulation of debris flows in erodible channels. Comput Geosci 35(5): 993–1006. https://doi.org/10.1016/j.cageo.2007.11.008

Berti M, Simoni A (2014) DFLOWZ: a free program to evaluate the area potentially inundated by a debris flow. Comput Geosci 67(2):14–23. https://doi.org/10.1016/j.cageo.2014.02.002

Bout B, Lombardo L, Westen CJV, Jetten VG (2018) Integration of two-phase solid fluid equations in a catchment model for flashfloods, debris flows and shallow slope failures. Environ Model Softw 105:1–16. https://doi.org/10.1016/j.envsoft.2018.03.017

Chang M, Tang C, Van Asch TWJ, Cai F (2017) Hazard assessment of debris flows in the Wenchuan earthquake-stricken area, South West China. Landslides 14:1783–1792. https://doi.org/10.1007/s10346-017-0824-9

Chen H, Lee CF (2000) Numerical simulation of debris flow. Can Geotech J 37(1):146–160. https://doi.org/10.1139/t99-089

Chen XQ, Cui P, You Y, Chen JG, Li DJ (2015a) Engineering measures for debris flow hazard mitigation in the Wenchuan earthquake area. Eng Geol 194:73–85. https://doi.org/10.1016/j.enggeo.2014.10.002

Chen XZ, Chen H, Yong Y, Liu JF (2015b) Susceptibility assessment of debris flows using the analytic hierarchy process method-a case study in Subao river valley, China. J Rock Mech Geotech Eng 7(4):404–410. https://doi.org/10.1016/j.jrmge.2015.04.003

Chen HX, Zhang S, Peng M, Zhang LM (2016) A physically-based multi-hazard risk assessment platform for regional rainfall-induced slope failures and debris flows. Eng Geol 203:15–29. https://doi.org/10.1016/j.enggeo.2015.12.009

Cui P, Hu KH, Zhuang JQ, Yang Y, Zhang J (2011) Prediction of debris-flow danger area by combining hydrological and inundation simulation methods. J Mt Sci 8(1):1–9. https://doi.org/10.1007/s11629-011-2040-8

Cutter SL, Boruff BJ, Shirley WL (2003) Social vulnerability to environmental hazards. Soc Sci Q 84(2):242–261

Dahal RK, Hasegawa S, Nonomura A, Yamanaka M, Masuda T, Nishino K (2009) Failure characteristics of rainfall-induced shallow landslides in granitic terrains of Shikoku Island of Japan. Environ Geol 56(7):1295–1310. https://doi.org/10.1007/s00254-008-1228-x

Degetto M, Gregoretti C, Bernard M (2015) Comparative analysis of the differences between using LiDAR contour-based DEMs for hydrological modeling of runoff generating debris flows in the Dolomites. Front Earth Sci 3:21. https://doi.org/10.3389/feart.2015.00021

Eidsvig UMK, Papathoma-Köhle M, Du DJ, Glade T, Vangelsten BV (2014) Quantification of model uncertainty in debris flow vulnerability assessment. Eng Geol 181:15–26. https://doi.org/10.1016/j.enggeo.2014.08.006

Fiebiger G (1997) Hazard mapping in Austria. J Torrent, Avalanche, Landslide and Rockfall Eng 134(61):93–104

Fuchs S, Heiss K, Hübl J (2007) Towards an empirical vulnerability function for use in debris flow risk assessment. Nat Hazards Earth Syst Sci 7:495–506

Gao L, Zhang M, Chen HX, Shen P (2016) Simulating debris flow mobility in urban settings. Eng Geol 214:67–78. https://doi.org/10.1016/j.enggeo.2016.10.001

Gentile F, Bisantino T, Liuzzi GT (2008) Debris-flow risk analysis in south Gargano watersheds (Southern-Italy), Nat. Hazards 44:1–17. https://doi.org/10.1007/s11069-007-9139-9

Giuseppe TA, Giovanni B, Giuseppina B, Ernesto C, Stefania L (2012) Assessment and mapping of debris-flow risk in a small catchment in eastern Sicily through integrated numerical simulations and GIS. Phys Chem Earth 49:52–63. https://doi.org/10.1016/j.pce.2012.04.002

Gregoretti C, Degetto M, Boreggio M (2016) GIS-based cell model for simulating debris flow runout on a fan. J Hydrol 534:326–340. https://doi.org/10.1016/j.jhydrol.2015.12.054

Himmelsbach I, Glaser R, Schoenbein J, Riemann D, Martin B (2015) Reconstruction of flood events based on documentary data and transnational flood risk analysis of the Upper Rhine and its French and German tributaries since AD 1480. Hydrol Earth Syst Sci 19(10):4149–4164. https://doi.org/10.5194/hess-19-4149-2015

Hu W, Dong XJ, Wang GH, van Asch TWJ, Hicher PY (2016) Initiation processes for run-off generated debris flows in the Wenchuan earthquake area of China. Geomorphology. 253:468–477. https://doi.org/10.1016/j.geomorph.2015.10.024

Hungr O (1995) A model for the runout analysis of rapid flow slides, debris flows and avalanches. Can Geotech J 32:610–623. https://doi.org/10.1139/cgj-2015-0481

Hurlimann M, Copons R, Altimir J (2006) Detailed debris flow hazard assessment in Andorra: a multidisciplinary approach. Geomorphology. 78:3–4. https://doi.org/10.1016/j.geomorph.2006.02.003

Imaizumi F, Sidle RC, Tsuchiya S, Ohsaka O (2006) Hydrogeomorphic processes in a steep debris flow initiation zone. Geophys Res Lett 33:L10404. https://doi.org/10.1029/2006GL026250

Iverson RM, Ouyang CJ (2015) Entrainment of bed material by Earth-surface mass flows: review and reformulation of depth-integrated theory. Rev Geophys 53(1):27–58. https://doi.org/10.1002/2013RG000447

Iverson RM, Reid ME, Logan M, Lahusen RG, Godt JW, Griswold JP (2011) Positive feedback and momentum growth during debris-flow entrainment of wet bed sediment. Nat Geosci 4(2):116–121. https://doi.org/10.1038/ngeo1040

Jakob M, Stein D, Ulmi M (2012) Vulnerability of buildings to debris flow impact. Nat Hazards 60(2):241–261. https://doi.org/10.1007/s11069-011-0007-2

Jinsoo K, Chuluong C, Soyoung P (2013) GIS-based landslide susceptibility analyses and cross-validation using a probabilistic model on two test areas in Korea. Disaster Adv 6(10):45–54

Kang S, Lee SR (2018) Debris flow susceptibility assessment based on an empirical approach in the central region of South Korea. Geomorphology. 308:1–12. https://doi.org/10.1016/j.geomorph.2018.01.025

Kwan JSH, Hui THH, Ho KKS (2013) Modelling the motion of mobile debris flows in Hong Kong. Landslide Science and Practice. Springer, Berlin, pp 29–35

Liang WJ, Zhuang DF, Jiang D, Pan JJ, Ren HY (2012) Assessment of debris flow hazards using a Bayesian network. Geomorphology. 171(9):94–100. https://doi.org/10.1016/j.geomorph.2012.05.008

Lin JY, Yang MD, Lin BR, Lin PS (2011) Risk assessment of debris flows in Songhe Stream, Taiwan. Eng Geol 123:100–112. https://doi.org/10.1016/j.enggeo.2011.07.003

Liu XL, Lei JZ (2003) A method for assessing regional debris flow risk: an application in Zhaotong of Yunnan province (SW China). Geomorphology. 52(3):181–191. https://doi.org/10.1016/S0169-555X(02)00242-8

Liu KF, Li HC, Hsu YC (2009) Debris flow hazard assessment with numerical simulation. Nat Hazards 49(1):137–161. https://doi.org/10.1007/s11069-008-9285-8

Lo WC, Tsao TC, Hsu C, H. (2012) Building vulnerability to debris flows in Taiwan: a preliminary study. Nat Hazards 64(3):2107–2128

Luna BQ, Remaître A, Van Asch TW, Malet JP, Van Westen CJ (2012) Analysis of debris flow behavior with a one-dimensional run-out model incorporating entrainment. Eng Geol 128:63–75. https://doi.org/10.1016/j.enggeo.2011.04.007

Ma Y, Yu B, Wu FY, Zhang JN, Qi X (2011) Research on the disaster of debris flow of Bayi Gully, Longchi, Dujiangyan, Sichuan on August 13, 2010. J Sichuan Uni (Engineering Sci Edi) 43(s1):92–98 (In Chinese)

Magirl CS, Griffiths PG, Webb RH (2010) Analyzing debris flows with the statistically calibrated empirical model LAHARZ in southeastern Arizona, USA. Geomorphology. 119:111–120. https://doi.org/10.1016/j.geomorph.2010.02.022

McCoy SW, Kean JW, Coe JA, Tucker GE, Staley DM, Wasklewicz WA (2012) Sediment entrainment by debris flows: in situ measurements from the head waters of a steep catchment. J Geophys Res 117: F03016. https://doi.org/10.1029/2011JF002278

O'Brien JS (2004) FLO-2D user's manual version.

O'Brien JS, Julien PY, Fullerton WT (1993) Two-dimensional water flood and mudflow simulation. J Hydraul Eng 119(2):244–261. https://doi.org/10.1061/(ASCE)0733-9429(1993)119:2(244)

Ouyang CJ, He SM, Tang C (2015a) Numerical analysis of dynamics of debris flow over erodible beds in Wenchuan earthquake-induced area. Eng Geol 194:62–72. https://doi.org/10.1016/j.enggeo.2014.07.012

Ouyang CJ, He SM, Xu Q (2015b) MacCormack-TVD finite difference solution of dam-break hydraulics over erodible alluvial sediment. J Hydraul Eng 141(5):06014026. https://doi.org/10.1061/(ASCE)HY.1943-7900.0000986

Papathoma-Köhle M, Keiler M, Totschnig R, Glade T (2012) Improvement of vulnerability curves using data from extreme events: debris flow event in South Tyrol. Nat Hazards 64(3):2083–2105. https://doi.org/10.1007/s11069-012-0105-9

PRC National Standard GB/T 21010-2017 (2017) Current land use classification. China Standards Press, Beijing

Pudasaini SP (2016) A novel description of fluid flow in porous and debris materials. Eng.Geol. 202:62–73. https://doi.org/10.1016/j.enggeo.2015.12.023

Regione Sicilia (2004) Piano Stralcio di bacino per l'Assetto Idrogeologico della Regione Siciliana – Relazione generale. <http://88.53.214.52/ pai/>.

Romenski E, Toro EF (2004) Compressible two-phase flows: two-pressure models and numerical methods. J Sci Comput 13(3):403–416. https://doi.org/10.1007/s10915-009-9316-y

Shen YM, Chen TL, Xiao GJ (1984) Flood calculation manual of small watershed in Sichuan Province, China.

Sousa J, Voight B (1995) Multiple-pulsed debris avalanche emplacement at Mount St. Helens in 1980: Evidence from numerical continuum flow simulations. J Volcanol Geotherm Res 66:227–250. https://doi.org/10.1016/0377-0273(94)00067-Q

Spence RJS, Baxter PJ, Zuccaro G (2004) Building vulnerability and human casualty estimation for a pyroclastic flow: a model and its application to Vesuvius. J Volcanol Geotherm Res 133(1):321–343. https://doi.org/10.1016/S0377-0273(03)00405-0

Takahashi T (1980) Debris flow on prismatic open channel. J Hydraul Div ASCE 106(HY3):381–396

Takahashi T, Nakagawa H, Harada T, Yamashiki Y (1992) Routing debris flows with particle segregation. J Hydraul Eng 118(11):1490–1507. https://doi.org/10.1061/(ASCE)0733-9429(1992)118:11(1490)

Tang C, Rengers N, Asch TWJV, Yang YH (2011) Triggering conditions and depositional characteristics of a disastrous debris flow event in Zhouqu City, Gansu Province, northwestern China. Nat Hazards Earth Syst Sci 11(11):2903–2912. https://doi.org/10.5194/nhess-11-2903-2011

Tecca PR, Genevois R (2009) Field observations of the June 30, 2001 debris flow at Acquabona (Dolomites, Italy). Landslides. 6(1):39–45. https://doi.org/10.1007/s10346-009-0145-8

Tiranti D, Deangeli C (2015) Modeling of debris flow depositional patterns according to the catchment and sediment source area characteristics. Front Earth Sci 3:8. https://doi.org/10.3389/feart.2015.00008

Totschnig R, Fuchs S (2013) Mountain torrents: quantifying vulnerability and assessing uncertainties. Eng Geol 155(2):31–44. https://doi.org/10.1016/j.enggeo.2012.12.019

Totschnig R, Sedlacek W, Fuchs S (2011) A quantitative vulnerability function for fluvial sediment Transport. Nat Hazards 58:681–703. https://doi.org/10.1007/s11069-010-9623-5

United Nations, Department of Humanitarian Affairs (1991) Mitigating natural disasters: phenomena, effects and options—a manual for policymakers and planners. United Nations, New York.

Wang J, Yu Y, Yang S, Lu GH, Ou GQ (2014) A modified certainty coefficient method (M-CF) for debris flow susceptibility assessment: a case study for the Wenchuan earthquake meizoseismal areas. J Mt Sci 11(5):1286–1297. https://doi.org/10.1007/s11629-013-2781-7

Wang J, Yu Y, Wei XF, Gong QH, Xiong HX (2016) Run-out effects of debris flows based on numerical simulation. Open Civ Eng J 10: 859–869. https://doi.org/10.2174/1874149501610010859

Wei ZL, Xu YP, Sun HY, Xie W, Wu G (2018) Predicting the occurrence of channelized debris flow by an integrated cascading model: a case study of a small debris flow-prone catchment in Zhejiang Province, China. Geomorphology 308:78–90. https://doi.org/10.1016/j.geomorph.2018.01.027

Zhang SA, Zhang LM, Li XY, Xu LQ (2018) Physical vulnerability models for assessing building damage by debris flows. Eng Geol 247:145–158. https://doi.org/10.1016/j.enggeo.2018.10.017